Materials Advances

ROYAL SOCIETY OF CHEMISTRY

PAPER

View Article Online
View Journal | View Issue

Cite this: *Mater. Adv.*, 2023, 4, 2940

Cellulose-based fluorescent films with anti-counterfeiting and UV shielding capabilities enabled by enamine bonds†

Yuhong Qiao,[ab] Youwei Ma,[b] Xiaomin Chen,[ab] Wenyao Guo,[a] Yulin Min,[a] Jinchen Fan *[ac] and Zixing Shi *[b]

Received 20th March 2023,
Accepted 5th June 2023

DOI: 10.1039/d3ma00132f

rsc.li/materials-advances

Natural cellulose-based materials with multifunctionality are highly pursued and yet a scientific challenge. To this end, fluorescent polymer films with UV shielding and anti-counterfeiting abilities were designed by grafting microcrystalline celluloses with acetoacetyl groups followed by a cross-linking treatment with polyetherimide. After the cross-linking process, the mechanical properties of the polymer films were improved, and they produced enamine linkages, which can effectively prevent the transmittance of ultraviolet light and emit fluorescence. The crosslinked films completely shielded all wavelengths of UV. On account of the dynamic nature of the enamine bonds, the polymer films can be de-cross-linked and recycled. The fluorescence of the polymer film can be quenched by Cr(VI) solution, through which the film can be applied in the anti-counterfeiting area. Considering the wide accessibility of the cellulose, and the multifunctionality of our designed cellulose-based polymers, we believe that they have the potential for application on a large scale.

1. Introduction

Ultraviolet (UV) rays contribute to the development of some advanced technologies, such as ultraviolet spectrometry, photoetching, among others, and yet cause some damage to our health and materials in our daily lives. For example, ultraviolet radiation A (UVA, 315–400 nm) can penetrate and reach the deep layer of the skin, bringing about tanning and photoaging, and ultraviolet radiation B (UVB, 280–315 nm) mainly affects the skin's epidermal cells. Long-term exposure to UV light will lead to skin cancer in human beings and aging problems in polymer materials.[1,2] Therefore, it is rather urgent and important to develop materials with good UV shielding function across industries and academia.[3]

Generally, UV shielding polymers are prepared by incorporating inorganic nanoparticles such as graphene oxide,[3] titanium dioxide,[4] silicon dioxide,[5] among others, as the UV absorbers into the polymers. However, most inorganic nanoparticles exhibit photocatalysis and degrade the polymers to some extent.[6] Moreover, poor dispersion and aggregation issue of the nanoparticles in the polymers give rise to non-uniform UV shielding ability, limiting the wide applications of the polymers.[7] Some other researchers prepared UV shielding films by blending organic UV absorbers (lignin,[8] modified nanocellulose,[9] *etc.*) with polymers. For example, Ma reported the preparation of ultraviolet-shielding films by combining PVA with nano lignin composites.[10] Although it is very simple to prepare UV shielding films by the blending method, this method will face problems such as absorption precipitation, which will lead to poor shielding ability and pollution of other substances. Therefore, designing UV shielding polymers with stable, long duration and uniform UV shielding ability is challenging and highly desired.[11]

As one of the most abundant natural polymers on earth, cellulose is easy to obtain, biodegradable, and has excellent mechanical properties.[12] It is regarded as a promising green material, which can potentially serve as a matrix for UV shielding materials.[13,14] In recent years, the preparation of cellulose-based UV shielding materials was intensively explored and saw great progress.[9,15,16] For example, Zhang *et al.* have reported the preparation of UV shielding materials by mixing different UV absorbents into cellulose.[17–19] However, incorporation of UV absorbers would affect the transparency of the materials, negatively affecting the appearance and applications of the materials.[18] Compared to the physical blending with the UV absorbers, chemical modification of the cellulose with UV shielding motifs is more effective since the chemical attachment of UV shielding motifs is more stable, and the motif can be dispersed in the cellulose at a molecular level.[20,21]

[a] *College of Environmental and Chemical Engineering, Shanghai University of Electric Power, Shanghai, 200090, China. E-mail: jcfan@usst.edu.cn*
[b] *School of Chemistry & Chemical Engineering, State Key Laboratory for Metal Matrix Composite Materials, Shanghai Jiao Tong University, Shanghai 200240, China. E-mail: zxshi@sjtu.edu.cn*
[c] *School of Materials and Chemistry, University of Shanghai for Science and Technology, Shanghai, 200093, China*

† Electronic supplementary information (ESI) available. See DOI: https://doi.org/10.1039/d3ma00132f

Thanks to the polyhydroxy structure, cellulose can be chemically modified in several ways. Thereinto, through transesterification of the hydroxyl groups with *tert*-butyl acetoacetate (*t*-BAA) using thermal treatment, the highly reactive β-dicarbonyl group can be incorporated into the sidechain of the cellulose.[22–24] Then, the reaction of β-dicarbonyl and amines produces enamine bonds.[25] According to Liu *et al.*, a functional polymer film capable of UV shielding was prepared by introducing a conjugated (O═C–C═C–) structure into PVA and cellulose using the Hantzsch reaction.[25–27] Thus, we prepare films with UV shielding by introducing the ketoenamine structure (O═C–C═C–N–) into cellulose using the enamine reaction. At the same time, the conjugated structure exhibits good UV absorption performance, and the rigid microenvironment provided by semi-rigid cellulose chains and intermolecular interactions minimizes the non-radiative transition and can emit fluorescence under ultraviolet irradiation.[28,29]

Here, we developed a transparent, fluorescent cellulose-based UV barrier film through two steps (Scheme 1a): (1) transesterification of the hydroxyl groups in the presence of excess *t*-BAA (300 mol%) at 110 °C to produce acetoacetate cellulose (CAA) (synthesis mechanism in Scheme S1a, ESI†), (2) cross-linking of the CAA with different molecular weights of polyetherimides (PEA) to form the cross-linked film (CAA-PEA*x*, x: D230, D400, D2000) (synthesis mechanism shown in Scheme S1b, ESI†). The β-dicarbonyl group on CAA reacts with the amine group on PEA. The generation of enamine bonds imparts dynamic enamine bonds, and the resultant CAA-PEA*x* with fluorescence.[30] Leveraging the dynamic feature of enamine bonds, the cross-linked CAA-PEA*x* can be recycled using HCl solution due to the dissociation of enamine bonds.[31,32] The introduction of Cr(VI) can quench the fluorescence of CAA-PEA*x*, so Cr(VI) solution is used to treat the film to prepare the anti-counterfeiting pattern (Scheme 1b).

2. Experimental

2.1. Materials

Microcrystalline cellulose (MCC) provided by Angie Chemical Reagent Co., Ltd, was dried in a vacuum oven at 80 °C for

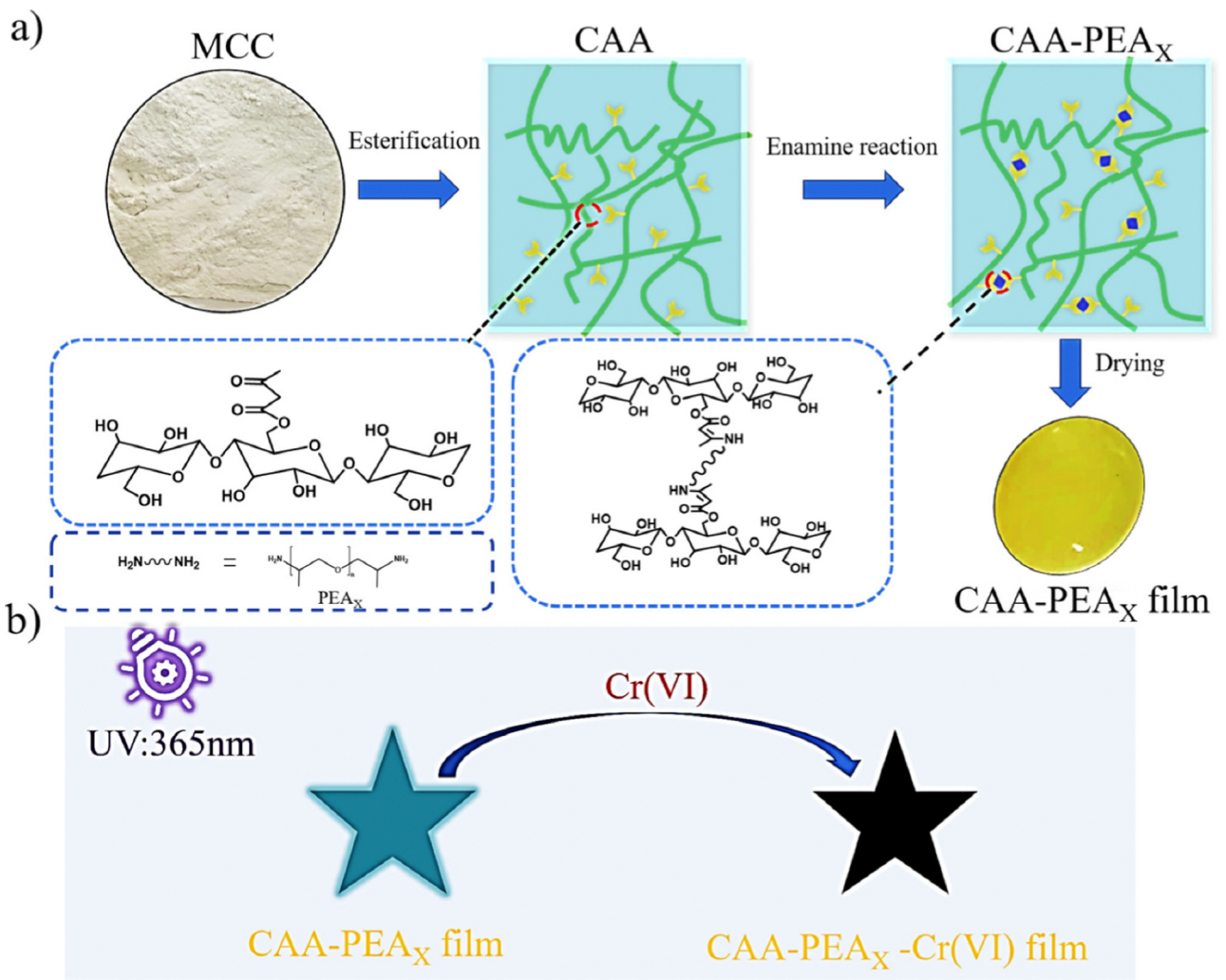

Scheme 1 (a) Synthesis of the cross-linked cellulose-based film (CAA-PEA*x*), and (b) schematic diagram of fluorescence quenching of CAA-PEA*x* by Cr(VI) at 365 nm UV light.

2 hours before use. Lithium chloride, polyetherimide (PEA, M_n = 230, 400, 2000 g mol^{-1}), *tert*-butyl acetoacetate (*t*-BAA) (95%), and *N*-dimethylacetamide (DMAc, 99.9%) were purchased from Shanghai Titan Technology Co., Ltd. All other chemicals used were of analytical grade and can be used without further purification.

2.2. Preparation of acetoacetate cellulose (CAA)

tert-Butyl acetoacetate (*t*-BAA) could easily react with microcrystalline cellulose (MCC) in DMAc/LiCl without an additional catalyst (Scheme S1a, ESI†). The degree of substitution (DS) of CAA was regulated by controlling the molar ratio of cellulose anhydrous glucose ring (AGU) and *t*-BAA. Microcrystalline cellulose and LiCl were dried for 24 h at 60 °C in a vacuum oven before use. Cellulose ion solution was prepared by directly dissolving cellulose with DMAc/LiCl system as the solvent. First, 2.00 g of microcrystalline cellulose was added to 50 mL of DMAc in a nitrogen atmosphere and activated at 150 °C for 30 minutes. The temperature was reduced to 80 °C, 4 g of LiCl (200 wt%) was added, and stirred at 80 °C for 2 h. Finally, the solution was stirred at room temperature until the solution became clear and transparent. The dissolved cellulose solution was heated to 110 °C in a nitrogen atmosphere, 5.85 g (37.0 mmol) of *t*-BAA of *tert*-butyl acetoacetate was added during stirring, the reaction was stopped for 4 hours, then the product was separated with ethanol and washed repeatedly, and then cellulose acetoacetate (CAA, DS = 1.0) was obtained using vacuum drying at 60 °C for 24 hours.

2.3. Preparation of the cross-linked cellulose-based films (CAA-PEA*x*)

CAA was cross-linked by treatment of different molecular weights of polyetherimide (PEAx, M_n = 230, 400, 2000 g mol^{-1}) to obtain the cross-linked cellulose-based films (CAA-PEA*x*) (Scheme S1b, ESI†). The obtained CAA (1 g) after the above procedures was first dissolved in 10 mL of DMSO, and PEAx was

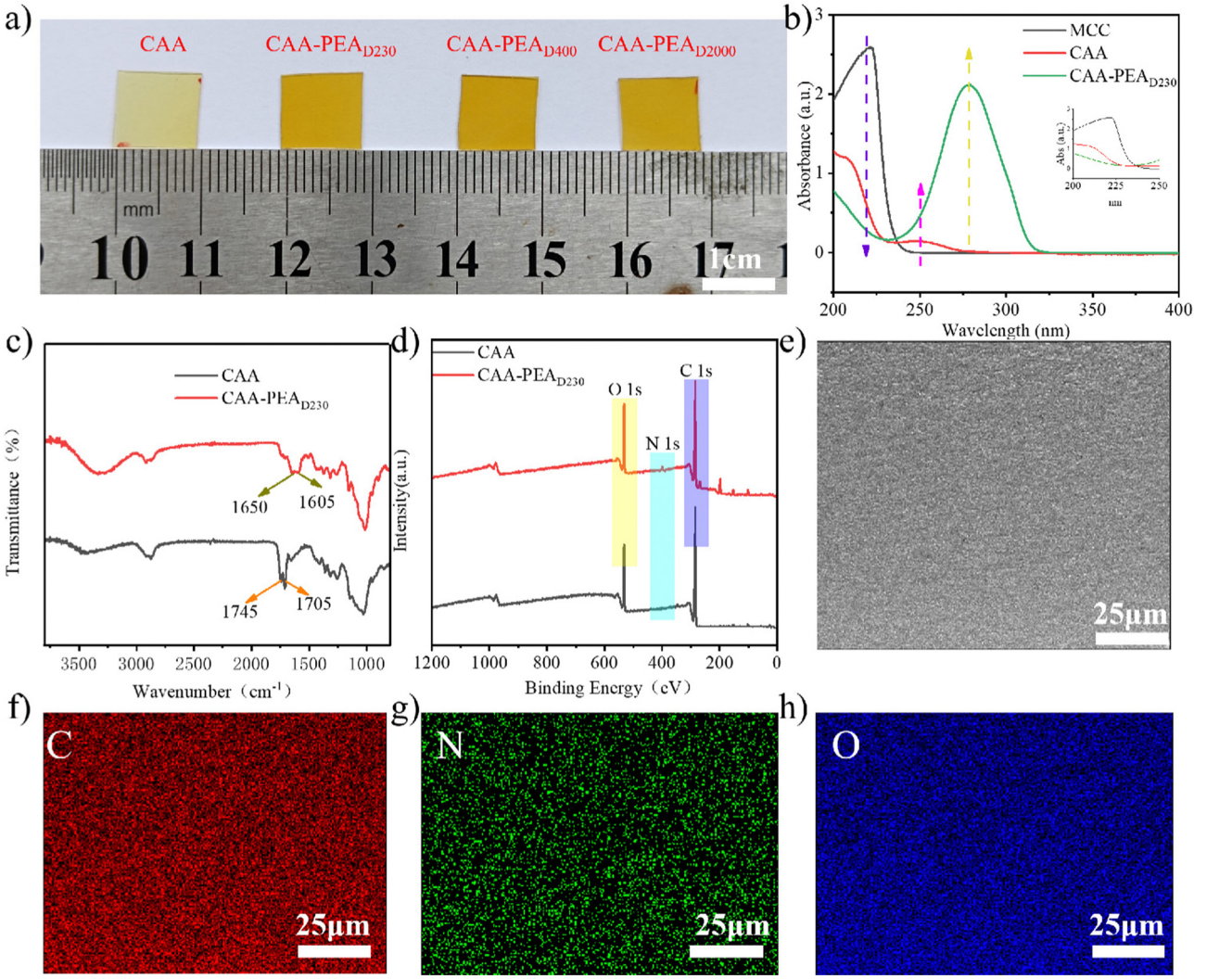

Fig. 1 (a) Optical images of cellulose acetoacetate film and film obtained by adding different polyether amines, (b) UV-vis absorption spectra of MCC, CAA and CAA-PEA$_{D230}$ films, (c) FT-IR spectra and (d) XPS wide-scan spectra of the CAA film and the CAA-PEA$_{D230}$ film, (e) SEM diagrams of cross sections of the CAA-PEA$_{D230}$ film, (f–h) EDS elemental mapping images C, N, O of the CAA-PEA$_{D230}$ film.

added to the CAA solution and stirred for 10 min. The mixture was casted onto a PTFE dish and dried in a drying oven at 60 °C for 2 days to obtain the PEA cross-linked cellulose film (CAA-PEA*x*). Here, *x* refers to the molecular weight of the PEA being used.

2.4. Characterization

Nuclear magnetic resonance hydrogen spectroscopy (^{1}H-NMR) was measured at room temperature using an AVANCE III HD500 produced by Bruker, Germany. The measurement specification is that the 10 mg product is dissolved in 0.5 mL of deuterated dimethyl sulfoxide (deuterated DMSO-d_6) in a nuclear magnetic tube. X-Ray photoelectron spectroscopy (XPS) was carried out using an electron spectrometer (AXISUltraDLD, Kratos, UK). X-Ray diffraction (XRD) spectra were determined on D8 DaVinci (Bruck, Germany). Fourier transform infrared (FT-IR) spectroscopy was carried out using the Spectrum100 model made by PerkinElmer Company in the United States using the attenuated reflectance (ATR) method. The optical tests of the film were performed on the UV 2550 Ultraviolet-visible spectrometer manufactured by Shimadzu in Japan. The cross-sectional morphology of the film was observed using a SEM. The steady-state fluorescence spectra are measured under controlled conditions on a Luminescence Spectrometer (LS 55). Thermogravimetric analysis (TGA) curves are measured using a DiscoveryTGA550 equipment. The sample is heated from 50 °C to 700 °C at a heating rate of 10 °C min^{-1}.

The degree of substitution (DS) of CAA was calculated according to eqn (1) as follows:

$$DS = (I_1 \times 7)/(I_2 \times 3) \quad (1)$$

where I_1 is the integral value of methyl acetoacetate and I_2 is the integral value of the dehydrated glucose ring skeleton of CAA.

2.5. Tensile test

The tensile test is carried out by using an Instron 3365 electronic universal material testing machine produced by Instron Company in the United States. Before testing, the sample is cut into a dumbbell sample using a cutting knife. According to the national standard GB/T 528, the total length of the sample is 50 mm, and the width in the middle is 4 mm. During the testing process, each group of parallel samples is measured at least three times, the tensile rate is 50 mm min^{-1}, and Young's modulus is obtained according to the slope of the elastic zone at the beginning of the stress–strain curve.

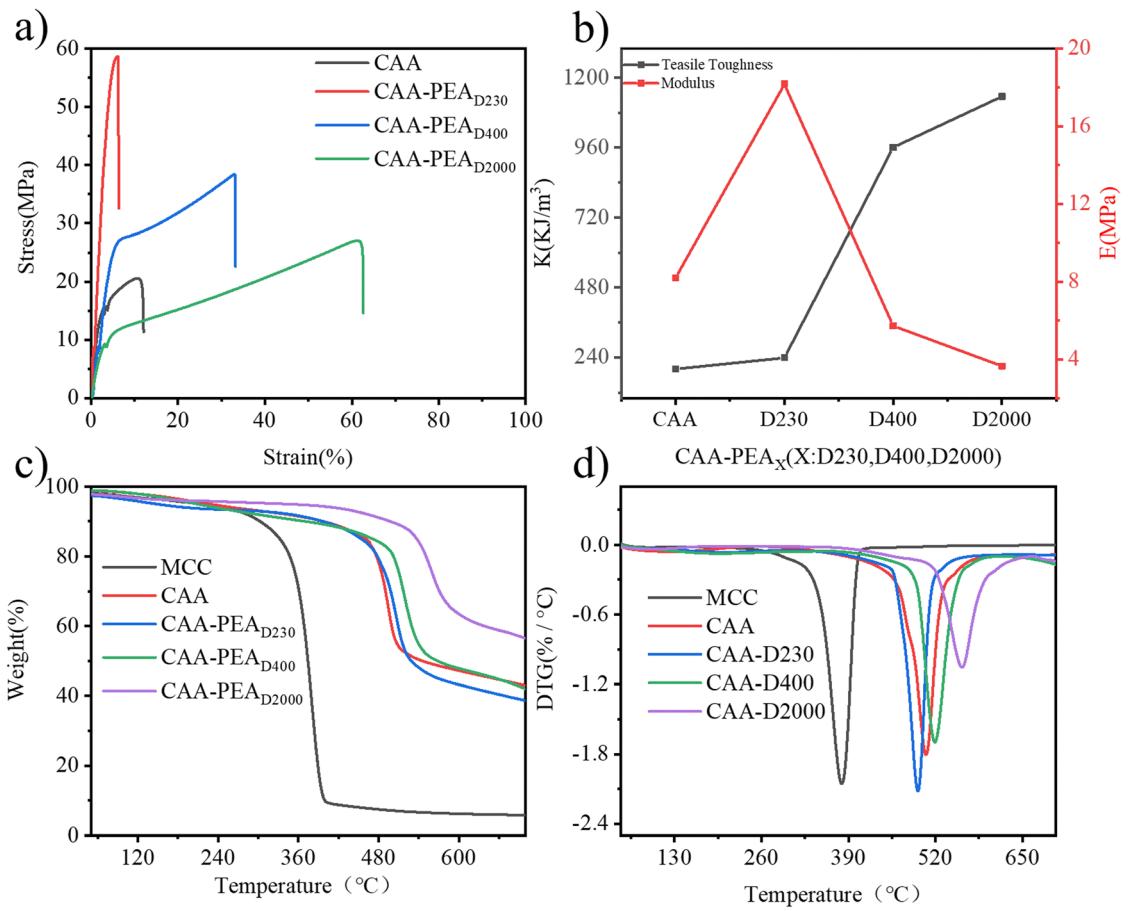

Fig. 2 Characterization and properties of the film: (a) stress–strain curves (b) corresponding mechanical parameters (c) TG and (d) DTG curves of the cellulose, CAA film, and CAA-PEA*x* film.

3. Results and discussion

3.1. Synthesis and characterization of fluorescent cellulose films

We observed the appearance of CAA and CAA-PEA*x* leveraging optical microscopy. The optical images of CAA-PEA*x* are shown in Fig. 1a. In visible light, the membranes of CAA, CAA-PEA$_{D230}$, CAA-PEA$_{D400}$, and CAA-PEA$_{D2000}$ appear light yellow. Ultraviolet (UV) absorption spectra, Fourier transform infrared (FT-IR) spectra, proton nuclear magnetic resonance (^{1}H-NMR) spectroscopy, and X-ray photoelectron spectroscopy (XPS) spectra of cellulose, the CAA film, and the CAA-PEA*x* film were conducted to further investigate the chemical evolution during the process. The UV absorption peak of the CAA-PEA film showed obvious redshift compared with that of the CAA film, and the absorption intensity was significantly enhanced, which was attributed to the formation of ketoenamine structures (Fig. 1b). Based on the FT-IR spectra (Fig. S1, ESI†) of the CAA film and the MCC film, esterification of the cellulose hydroxyl groups can be confirmed by new peaks at 1705 and 1745 cm^{-1}, which were assigned to the stretching vibrations of the acetoacetyl moiety. Furthermore, compared with the CAA film, the FT-IR spectra of the CAA-PEA$_{D230}$ film exhibited two new peaks at 1650 and 1605 cm^{-1}, which could be attributed to enylamine bonds (Fig. 1c). The same change can be seen in other cases (Fig. S2, ESI†), among which CAA reacts with different molecular weights of PEA. In Fig. 1d, the XPS spectra of CAA and CAA-PEA$_{D230}$ films present two representative peaks for O 1s and C 1s. But there is a new signal at 396 eV assigned to N 1s emerged in the XPS spectra of CAA-PEA$_{D230}$, which also supports the formation of the enamine bond in the CAA-PEA$_{D230}$ (Fig. 1d). As shown in the SEM image in Fig. S4 (ESI†), the CAA, CAA-PEA$_{D230}$, CAA-PEA$_{D400}$, and CAA-PEA$_{D2000}$ films show a smooth cross-section. Additionally, the energy-dispersive spectroscopy (EDS) mapping images of the CAA-PEA$_{D230}$ film showed a uniform distribution of C, N and O elements (Fig. 1e–h), further suggesting that the enamine bond was anchored homogeneously in uniformly anchored cellulose.

The structure of CAA-PEA*x* was further explored by X-ray diffractometry (XRD). The UV absorbing ability induced by the enamine bond enables CAA-PEA$_{D230}$ to function as the UV shielding material. The XRD spectra show that MCC has two sharp peaks at $2\theta = 15^\circ$ and 23°, suggesting its strong crystalline ability (Fig. S3a, ESI†). After the modification and cross-linking treatment, the two sharp peaks gradually weaken in the spectra of CAA and finally turn into a broad peak in that of CAA-PEA*x* (Fig. S3, ESI†), strongly supporting an amorphous structure in CAA-PEA*x*. The results indicate that the incorporation of both β-dicarbonyl groups and cross-linker PEA break down the crystallinity of MCC.

3.2. Mechanical properties of CAA-PEA*x*

Mechanical properties can be tailored by introducing different polyether amines. In Fig. 2a, it can be seen that the elongation at the break of the film increased from 6% to 61.5%, and the breaking strength decreased from 58.6 MPa to 27 MPa. The modulus and tensile strength of CAA and CAA-PEA*x* films are calculated and summarized in Fig. 2. The modulus of the CAA

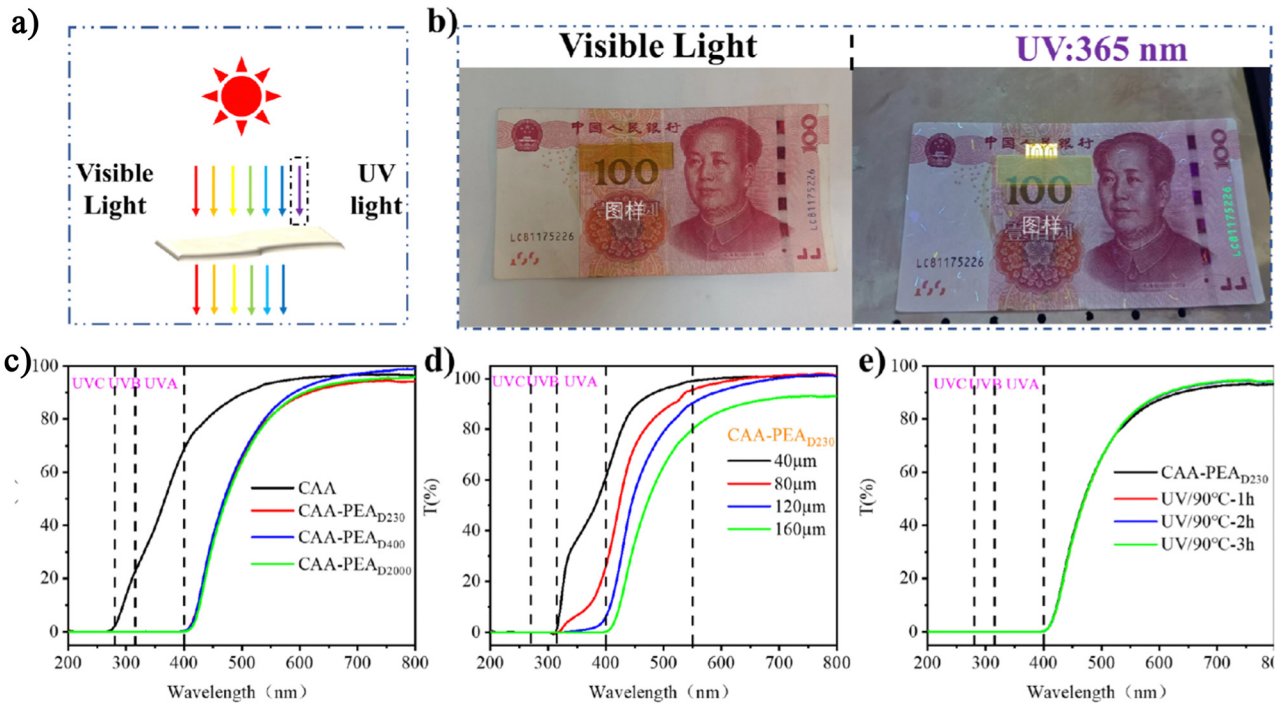

Fig. 3 (a) UV shielding schematic diagram, (b) photos of CAA-PEA$_{D230}$ film under UV (365 nm) and visible light, (c) UV-visible transmittance curves of CAA, CAA-PEA$_{D230}$, CAA-PEA$_{D400}$, and CAA-PEA$_{D2000}$ films, (d) UV-visible transmittance curves of CAA-PEA$_{D230}$ film with different thickness, and (e) UV-visible transmittance curves of the modified film irradiated with high power UV (365 nm) at 90 °C for different times.

film is 490 MPa, the modulus of the CAA-PEAD230 film is almost 2.5 times that of the CAA film, and the modulus of the CAA-PEAD400 and CAA-PEAD2000 films is slightly lower than the CAA film, the tensile strength of the CAA-PEA*x* film is stronger than the CAA film (Fig. 2b). First of all, it can be seen in Fig. S5a (ESI†) that the elongation at break of CAA decreases from 14% to 7% with the increase of *t*-BAA, and the fracture strength increases from 20 MPa to 34 MPa. By calculating the modulus of the film, the modulus of the film increases from 7.4 MPa to 8.0 MPa with the increase of the degree of acetylation (Fig. S5b, ESI†). The change of CAA elongation at break may be related to the degree of acetylation of cellulose. With the deepening of acetylation, the rigidity of the film can be attributed to the increase of side chains and the formation of new hydrogen bonds between diketones and cellulose. The stress-strain curve of the CAA-PEA_{D230} film as a function of the PEA_{D230} content is shown in Fig. S5c (ESI†). The change of its modulus is calculated as shown in Fig. S5d (ESI†). The amount of PEA_{D230} in the CAA-PEA_{D230} increased from 5% to 15%, and the modulus of the film increased from 6.6 MPa to 8.4 MPa, which is attributed to the increase of cross-linking points leading to the increase of cross-linking density and making the cross-linking network denser. In addition, thermogravimetric (TG) analysis and differential thermogravimetric (DTG) analysis show that the film had good thermal stability (Fig. 2c and d). The initial decomposition temperature of the CAA film is about 480 °C. The initial decomposition temperature of the CAA-PEA*x* film is basically the same as that of the CAA film, indicating that mild homogeneous modification does not affect the thermal properties of the CAA film. However, the thermal stability of the modified cellulose is better than that of the unmodified cellulose. The pyrolysis temperature of the modified cellulose is higher than that of the unmodified cellulose because the increase of the side chain leads to the increase of the pyrolysis temperature. At the same time, the thermal stability of polyether amines is changed by changing the type of polyether amines. As can be seen from Fig. 2c and d, the thermal stability of polyether amines is improved with the increase of molecular weight. The reason may be that the introduction of longer alkyl chains leads to the improvement of the thermal stability of the film.

3.3. Ultraviolet shielding property of CAA-PEA*x*

A film with a UV shielding function is widely used in life. The preparation of materials that only shield UV and have high transmittance in the visible range has a wider range of application scenarios (Fig. 3a). The CAA-PEA*x* film prepared by us has high transparency and excellent UV shielding ability, which greatly expands its application. The UV blocking performance of CAA-PEA_{D230} was tested using the paper money security code,

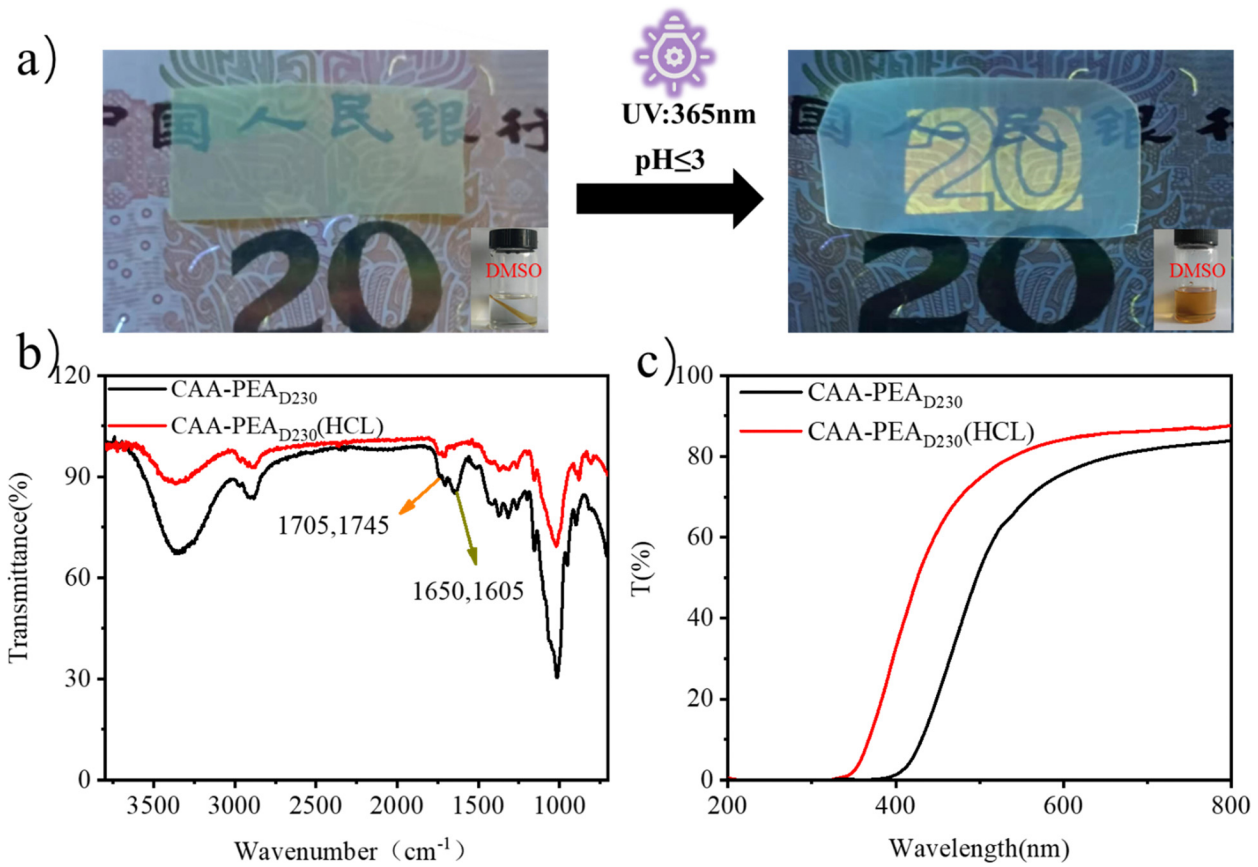

Fig. 4 (a) Photograph of UV shielding function and solubility of the film before and after HCl solution, (b) FT-IR spectra and (c) UV-visible transmittance curves of the film before and after acidolysis.

and the UV blocking ability of the plastic sheet was intuitively demonstrated. First of all, we can clearly see the numbers under the banknotes under visible light, which indicates that the CAA film has good light transmittance (Fig. 3b). Under UV lamp (365 nm) irradiation, the security code blocked by the film on the banknotes cannot be shown at all, while the unblocked part can be shown, which indicates that CAA-PEA$_{D230}$ has excellent UV shielding ability (Fig. 3b). The UV-visible transmittance of CAA and CAA-PEA$_{D230}$ films (thickness is about 160 μm) is measured in the wavelength range of 200–800 nm. As shown in Fig. 3c, the original CAA film shows high transparency, about 95%. In addition, the CAA film has a good shielding effect on UVC band ultraviolet light, but it is not obvious for UVA and UVB band ultraviolet light shielding effect. This shows that the CAA film does not have effective UV protection. However, the CAA-PEA (D230, D400, and D2000) film shows excellent UV-blocking properties, which can block ultraviolet light at all wavelengths. Although the addition of polyetherimide has some effect on the transmittance of visible light, it still has good optical properties (the transmittance at 550 nm is 80%). The thickness of the thin film is also an important index affecting its optical properties. As shown in Fig. 3d, the UV shielding ability of the CAA-PEA$_{D230}$ film varies significantly by changing the thickness of the film. When the thickness of the film is 40 and 80 μm, it only has a 100% shielding effect on UVB and UVC, and a poor shielding effect on ultraviolet light in the UVC band. The UV shielding effect is improved with the increase in thickness. When the thickness reaches 160 μm, the ultraviolet light of all bands can be completely shielded. However, its visible light transmittance has decreased, but still

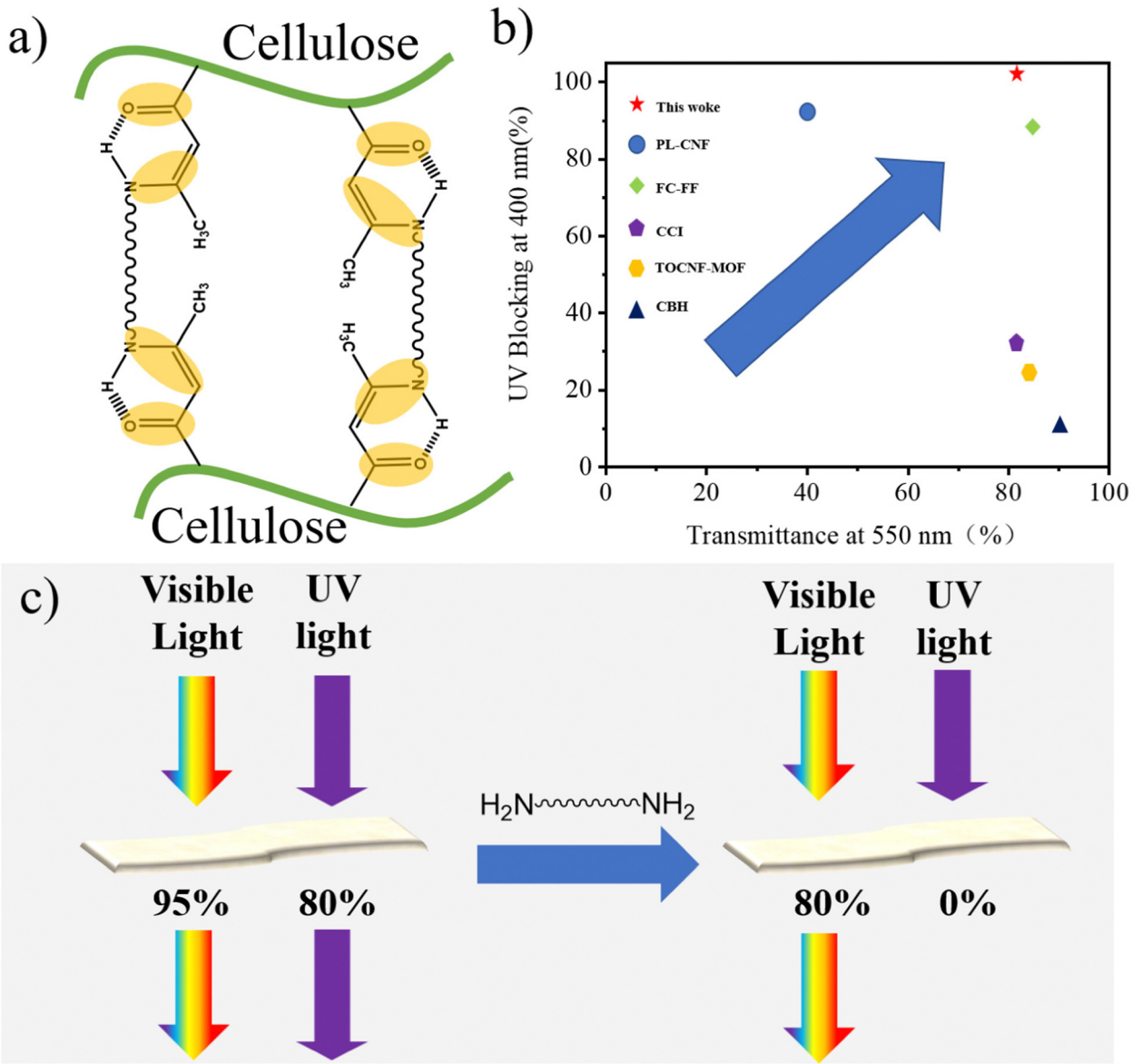

Fig. 5 (a) UV-blocking mechanism, (b) a comparison of the UV blocking and transparency of the CAA-PEA$_{D230}$ film with other Cellulose-based UV-shielding films, and (c) schematic showing the UV-filtering of the CAA-PEA film.

has a level of more than 80%. The service life of UV protective materials is also an important index. To monitor the effect of UV irradiation and temperature on UV barrier performance, the modified CAA film samples were irradiated under a 365 nm ultraviolet lamp at 90 °C. As shown in Fig. 3e, it still completely blocks UV light. The relationship between the content of the enamine bond and UV blocking performance at the same thickness is shown in Fig. S6 (ESI†). With the increase of the content of the enamine bond, the UV shielding performance increased with decreased transparency. But changes in transparency can be ignored.

Plastic products are widely used in our life. But a lot of plastic flows into the environment, causing huge pollution to the environment. Therefore, recycling and degradation of plastics have become the focus of current research. The excellent UV shielding properties of the cellulose-based film prepared in this study are mainly attributed to the conjugated (O=C–C=C–N–) molecular structure, and the enamine bond as a new dynamic bond will dissociate under acidic conditions. As shown in Fig. 4a, using the security code on the banknote, it can be clearly seen under the ultraviolet lamp that after being treated with HCl solution, the film's shielding ability to UV light (365 nm) becomes worse. At the same time, the destruction of the cross-linked network at pH $\leq$ 3 can re-dissolve the cellulose film, which facilitates sample recovery (Fig. 4a). The disappearance of peaks at 1650 and 1605 cm^{-1} of acid-treated cellulose film indicated the dissociation of enamine bonds by infrared spectroscopy (Fig. 4b). The dissociation of the enamine bond leads to the destruction of the conjugated structure. At the same time, the UV shielding ability of the film was measured, and it was found that the UV shielding ability decreased, while the transmittance increased in the visible

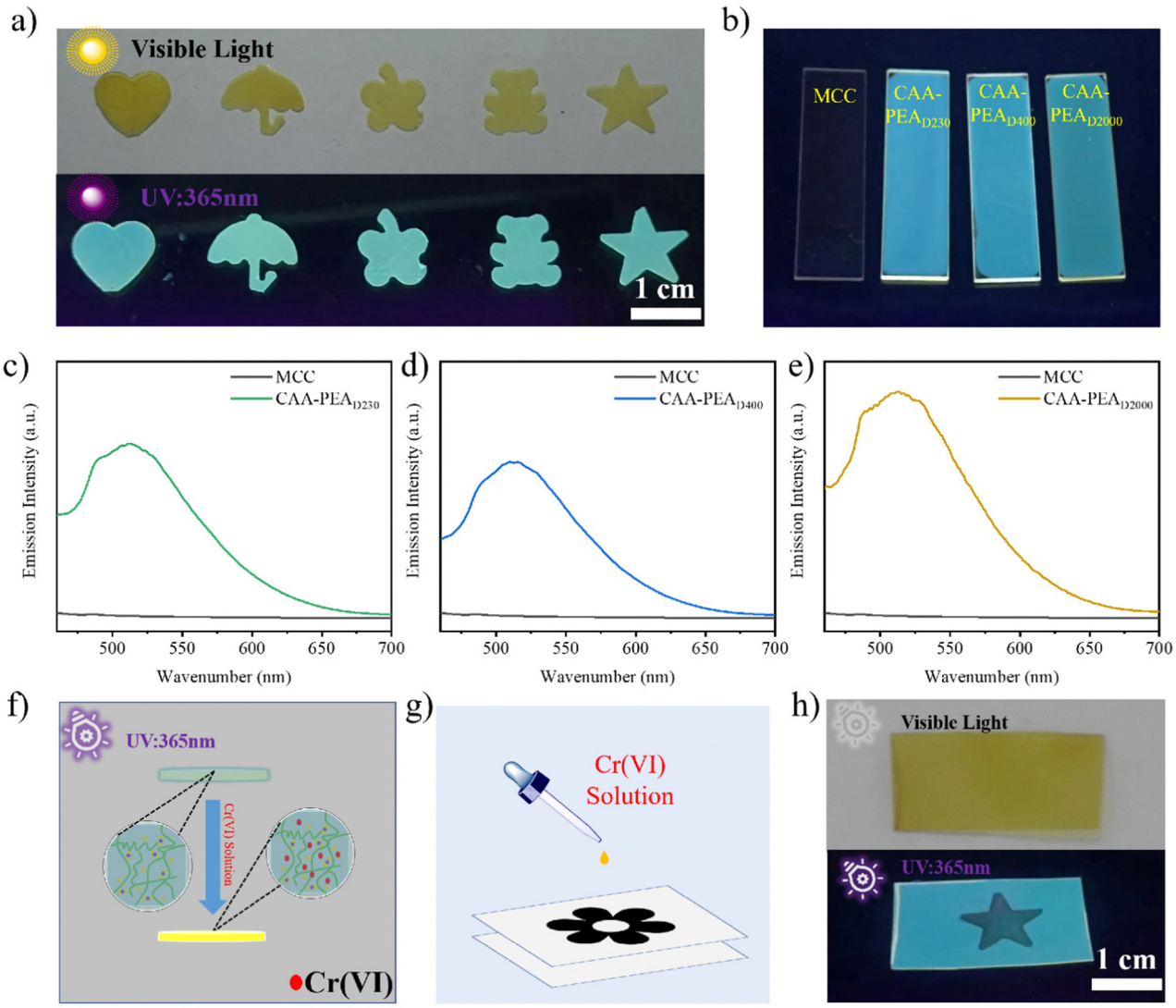

Fig. 6 (a) Digital photos of the CAA-PEAD230 film under visible light and 365 nm ultraviolet light, and (b) digital photos of the CAA-PEA$_{D230}$, CAA-PEA$_{D400}$, and CAA-PEAD$_{2000}$ films under 365 nm ultraviolet light, (c) emission spectra of the CAA-PEA$_{D230}$, (d) CAA-PEA$_{D400}$ and (e) CAA-PEA$_{D2000}$ films (λ_{Ex}: 350 nm), (f) schematic diagram of fluorescence quenching, (g) schematic diagram of pattern preparation using the dipping method, (h) intelligent pattern display of the CAA-PEA$_{D230}$ film.

range (Fig. 4c). This suggests that we can adjust its UV shielding by adjusting the pH.

The UV shielding mechanism is shown in Fig. 5a. The excellent UV shielding performance of the fluorescent film is mainly due to the conjugated (O═C–C═C–N–) molecular structure. It is reported that the conjugated structure shows good UV absorption properties. In the ground state, the molecule absorbs ultraviolet radiation and transitions to the excited state. However, the excited state of absorbing energy is unstable and will return to the ground state. Fig. 5b summarizes the reported transparency and UV shielding properties of the cellulose-based film.[14,27,33–35] The arrows in the picture show the trend of materials' comprehensive transparency and UV shielding properties. The CAA-PEA film in this work shows a good balance between excellent UV shielding and high transparency, which is much better than other films. Fig. 5c depicts a UV-blocking scheme based on the cellulose film. After the reaction of cellulose acetoacetate with the amino group, the modified film not only completely blocked ultraviolet radiation but also showed high transparency (80%). Therefore, the film has great application potential in the field of fluorescence and ultraviolet shielding.

3.4. Fluorescence properties

The optical image of the film is shown in Fig. 6a. Under visible light, the colour of the modified film is yellow and cyan fluorescence was observed under UV light (365 nm). This shows that the cellulose-based fluorescent film can be processed into different shapes using a simple cutting method. In addition, different polyether amines as cross-linking agents emit almost the same fluorescence under ultraviolet light (365 nm), while the MCC film does not appear without an obvious change (Fig. 6b). The excitation spectra measured with CAA-PEA$_{D230}$ as an example are shown in Fig. S7 (ESI†). The maximum excitation wavelength of the CAA-PEA$_{D230}$ film appeared from 275 to 375 nm. The emission spectra of the MCC and CAA-PEA*x* films are shown in Fig. 6c–e. It can be seen that the emission spectra of different CAA-PEA films show a wide peak between 460 nm and 650 nm. There are abundant hydrogen bonds in cellulose, which can make the configuration of the enaminone compounds more planar, thus inhibiting free rotation in the molecules and preventing energy dissipation in a non-radiative form. The introduction of conjugated structures (O═C–C═C–N–) gives cellulose film excellent UV absorption capacity, while converting part of the energy into fluorescence. At the same time, the prepared fluorescent film has excellent solvent resistance, and after one week of treatment with different solvents, the fluorescence emitted under ultraviolet light irradiation (365 nm) is the same as before treatment (Fig. S8, ESI†).

Through the secondary derivation of cellulose, the fluorescent materials of cellulose have excellent solvent resistance. Fluorescence can be quenched by introducing Cr(VI) (Fig. 6f). Therefore, we adopted a simple dip coating method (Fig. 6g) to obtain a fluorescent film with various security information by mask processing with different patterns (Fig. 6h). The fluorescence of CAA-PEA*x* can be quenched by the introduction of Cr(VI) possibly due to the electron transfer process under UV light.[36,37] Different security information can still be clearly expressed (Fig. S9, ESI†). Such excellent processability and formability make fluorescent cellulose films suitable for complex anti-counterfeiting, information encryption and storage, smart labels, packaging, detection sensors, and many other fields.

4. Conclusions

In summary, we prepared a new transparent, recyclable and tough cellulose-based UV-blocking fluorescent film by the reaction between the β-dicarbonyl and amine groups. Conjugated structure (O═C–C═C–N–) is uniformly distributed in the CAA-PEA film. The obtained film has a higher transparency. At the same time, the cross-linked structure of the film is dissociated under the condition of pH $\leq$ 3, which provides the possibility for sample recovery. Moreover, even after soaking in different solvents for 24 hours, the film still showed bright fluorescence emission under ultraviolet irradiation. More importantly, the conjugate structure (O═C–C═C–N–) gives the film excellent UV blocking properties, almost 100% shielding against UVA and UVB. In addition, the prepared film was found to be stable to ultraviolet radiation and high temperature (90 °C). This extraordinary performance makes it a promising application in many fields such as UV protection, anti-counterfeiting and packaging.

Conflicts of interest

The authors declare no conflict of interest.

Acknowledgements

The authors thank the National Nature Science Foundation of China (51873104, 51903153, 52073171) and the China Postdoctoral Science Foundation (2018M640382) for their financial support.

Notes and references

1 D. L. Narayanan, R. N. Saladi and J. L. Fox, *Int. J. Dermatol.*, 2010, **49**, 978–986.
2 R. Losantos, I. Funes-Ardoiz, J. Aguilera, E. Herrera-Ceballos, C. Garcia-Iriepa, P. J. Campos and D. Sampedro, *Angew. Chem., Int. Ed.*, 2017, **56**, 2632–2635.
3 X. F. Zhang, L. Song, Z. Wang, Y. Wang, L. Wan and J. Yao, *Int. J. Biol. Macromol.*, 2020, **145**, 663–667.
4 M. M. Abd El-Hady, A. Farouk, S. E. Saeed and S. Zaghloul, *Polymers*, 2021, **13**, 4027.
5 C. Zhang, C. Hu, S. Chang, J. Zhan, J. Shen and H. Shen, *Processes*, 2021, **10**, 6.
6 M. A. Nassar and A. M. Youssef, *Carbohydr. Polym.*, 2012, **89**, 269–274.
7 X. Zhang, W. Liu, D. Sun, J. Huang, X. Qiu, Z. Li and X. Wu, *ChemSusChem*, 2020, **13**, 4974–4984.

8 K. Shikinaka, M. Nakamura, R. R. Navarro and Y. Otsuka, *Green Chem.*, 2019, **21**, 498–502.
9 J. A. Sirviö, M. Visanko, J. P. Heiskanen and H. Liimatainen, *J. Mater. Chem. A*, 2016, **4**, 6368–6375.
10 W. Yang, H. Ding, G. Qi, C. Li, P. Xu, T. Zheng, X. Zhu, J. M. Kenny, D. Puglia and P. Ma, *React. Funct. Polym.*, 2021, **162**, 104873.
11 Y. Huang, J. C. Law, T. K. Lam and K. S. Leung, *Sci. Total Environ.*, 2021, **755**, 142486.
12 D. Klemm, B. Heublein, H. P. Fink and A. Bohn, *Angew. Chem., Int. Ed.*, 2005, **44**, 3358–3393.
13 R. Trovagunta, T. Zou, M. Osterberg, S. S. Kelley and N. Lavoine, *Carbohydr. Polym.*, 2021, **254**, 117480.
14 T. Yang, P. Xiao, J. Zhang, R. Jia, H. Nawaz, Z. Chen and J. Zhang, *ACS Appl. Mater. Interfaces*, 2019, **11**, 4302–4310.
15 K. Liu, H. Du, T. Zheng, H. Liu, M. Zhang, R. Zhang, H. Li, H. Xie, X. Zhang, M. Ma and C. Si, *Carbohydr. Polym.*, 2021, **259**, 117740.
16 Z. Huang, Z. Huang, L. Feng, X. Luo, P. Wu, L. Cui and X. Mao, *Carbohydr. Polym.*, 2018, **202**, 470–478.
17 J. Huang, Z. Lu, J. Li, D. Ning, Z. Jin, Q. Ma, L. Hua, E. Songfeng and M. Zhang, *Carbohydr. Polym.*, 2021, **255**, 117330.
18 Y. Wang, J. Su, T. Li, P. Ma, H. Bai, Y. Xie, M. Chen and W. Dong, *ACS Appl. Mater. Interfaces*, 2017, **9**, 36281–36289.
19 A. Ahmed, B. Adak, T. Bansala and S. Mukhopadhyay, *ACS Appl. Mater. Interfaces*, 2020, **12**, 1687–1697.
20 C. Lu, J. Yu, C. Wang, J. Wang and F. Chu, *Carbohydr. Polym.*, 2018, **188**, 128–135.
21 Y. Qi, S. Lin, J. Lan, Y. Zhan, J. Guo and J. Shang, *Carbohydr. Polym.*, 2021, **260**, 117760.
22 L. Rong, H. Liu, B. Wang, Z. Mao, H. Xu, L. Zhang, Y. Zhong, J. Yuan and X. Sui, *ACS Sustainable Chem. Eng.*, 2018, **6**, 9028–9036.
23 L. Guo, H. Liu, F. Peng and H. Qi, *Carbohydr. Polym.*, 2021, **274**, 118635.
24 H. Liu, L. Rong, B. Wang, R. Xie, X. Sui, H. Xu, L. Zhang, Y. Zhong and Z. Mao, *Carbohydr. Polym.*, 2017, **176**, 299–306.
25 B. Li, C. Xu, J. Yu, L. Liu, X. Zhang and Y. Fan, *Green Chem.*, 2023, 479–489.
26 H. Liu, H. Yang, K. Zhu, F. Peng, L. Guo and H. Qi, *Mater. Horiz.*, 2022, **9**, 815–824.
27 F. Peng, H. Liu, D. Xiao, L. Guo, F. Yue, H. Würfe, T. Heinze and H. Qi, *J. Mater. Chem. A*, 2022, **10**, 7811–7817.
28 L.-L. Du, B.-L. Jiang, X.-H. Chen, Y.-Z. Wang, L.-M. Zou, Y.-L. Liu, Y.-Y. Gong, C. Wei and W.-Z. Yuan, *Chin. J. Polym. Sci.*, 2019, **37**, 409–415.
29 M. Zeng, T. Li, Y. Liu, X. Lin, X. Zu, Y. Mu, L. Chen, Y. Huo and Y. Qin, *Chem. Eng. J.*, 2022, **446**, 1385–8947.
30 S. Virtanen, R. Talja and S. Vuoti, *Carbohydr. Polym.*, 2017, **177**, 105–115.
31 A. Sanchez-Sanchez, D. A. Fulton and J. A. Pomposo, *Chem. Commun.*, 2014, **50**, 1871–1874.
32 H. Liu, L. Rong, B. Wang, Z. Mao, R. Xie, H. Xu, L. Zhang, Y. Zhong and X. Sui, *Carbohydr. Polym.*, 2017, **170**, 117–123.
33 J. Wang, Y. Cao, B. Jaquet, C. Gerhard, W. Li, X. Xia, J. E. Rauschendorfer, P. Vana and K. Zhang, *ACS Appl. Mater. Interfaces*, 2021, **13**, 28668–28678.
34 J. Ou, S. Hu, L. Yao, Y. Chen, H. Qi and F. Yue, *Chem. Eng. J.*, 2023, **453**, 1385–8947.
35 F. Tan, L. Zha and Q. Zhou, *Adv. Mater.*, 2022, **34**, e2201470.
36 Q. Huang, Q. Bao, C. Wu, M. Hu, Y. Chen, L. Wang and W. Chen, *J. Pharm. Anal.*, 2022, **12**, 104–112.
37 Y. Sun, L. Xu, P. Jin, X. Bai, X. Jin and X. Shi, *Chem. Eng. J.*, 2021, **405**, 1385–8947.